Journal of Molecular Liquids 423 (2025) 126873

Contents lists available at ScienceDirect

Journal of Molecular Liquids

journal homepage: www.elsevier.com/locate/molliq

Energy-efficient nanobubble generation with microporous materials

Lingxi Ouyang [a,b], Haotian Cha [a,b], Jun Zhang [a,c], Helena H.W.B. Hansen [a,b], Qin Li [a,c], Beng Hau Tan [d], Porun Liu [b], Dongke Zhang [e], Liang Wang [b], Nam-Trung Nguyen [a,b,*], Hongjie An [a,b,*]

[a] Queensland Micro and Nanotechnology Centre, Griffith University, 170 Kessels Road, Nathan, QLD 4111, Australia
[b] School of Environment Science, Griffith University, 170 Kessels Road, Nathan, QLD 4111, Australia
[c] School of Engineering and Built Environment, Griffith University, 170 Kessels Road, Nathan, QLD 4111, Australia
[d] Shenzhen Institute for Advanced Study, University of Electronic Science and Technology of China, Shenzhen 518110, China
[e] Centre for Energy (M473), The University of Western Australia, 35 Stirling Highway, Crawley, WA 6009, Australia

ARTICLE INFO

Keywords:
Porous materials
Energy efficient
Oversaturation
Nanobubble
Nucleation
Carbon molecular sieves
Zeolite molecular sieves

ABSTRACT

The last decade has seen the ascendence of technologies based on micro- and nanobubbles for a wide range of applications, including, but not limited to, lake cleaning, aquaculture, and biomedicine. The bubble suspensions that mediate such technologies are often produced using methods that incur large amounts of energy as well as costs, such as through vigorous mechanical aeration and ultrasound. Here, we present a method to passively produce bubble suspensions with tuneable composition using microporous materials such as carbon and zeolite molecular sieves, leveraging on the high adsorption energy of such materials to create suspensions rich in dissolved gas. Apart from being energy efficient, this method distinguishes itself from commercial methods of producing bubble suspensions through its ability to control gas composition: carbon molecular sieves produce a suspension that is sparged of oxygen but nitrogen-rich, whereas zeolite molecular sieves produce the converse outcome. Our findings not only reduce barriers towards the commercialisation of technologies dependent on bubble suspensions but also invite significant new applications for bubble technologies in areas such as aquaculture or medicine, where there is still an unfulfilled demand to tune the chemical environment of bubble suspensions.

1. Introduction

The production of fine bubbles, liquid suspensions containing a vast amount of bubbles, is the centre for a more sustainable world [1]. Such bubbles, known industrially as ultrafine bubbles and in academic circles as nanobubbles, are already commercially deployed in diverse sectors to improve cleaning performance in washing machines [2,3], to revitalise lakes and large bodies of water saddled with eutrophication [4], agriculture, mining and many others [5–9]. The rapid emergence of this field is exemplified by the recent publication of internationally recognised ISO standards for fine bubble technology (ISO/TS 24217-1:2023). The vast economic potential of fine bubbles has stimulated significant interest in producing them at scale. However, nearly all major methods of producing bubble suspensions incur significant engineering effort and energy expenditure: subjecting liquids to high environmental pressure [10,11], compressing gas through liquid-immersed membranes [12], or the production of cavitation through ultrasound [13]. Apart from energy inefficiency, some potential applications of fine bubbles require gas selectivity. In the remediation of lakes, agriculture and medicine, it is specifically desirable to produce bubble suspensions that are rich in oxygen [14,15].

Bubbling is very often seen when a sponge is immersed in water. This motivated us to explore bubble nucleation using these pores scaled down to microns or nanoscales, with examples of molecular sieves commercially available to the public. Early studies on cavitation claimed that surface crevices contributed to cavitation nuclei as these sites favoured heterogeneous nucleation of bubbles [16]. Further, they grew through gas diffusion under oversaturation conditions and eventually detached [17]. However, the current use of porous materials for nanobubble generation has been largely limited to passive hydrodynamic processes, wherein porous membranes serve as nozzle systems to release nanobubbles by introducing compressed gas into the fluid [18]. Although

* Corresponding authors at: School of Environment Science, Griffith University, 170 Kessels Road, Nathan, QLD 4111, Australia.
E-mail addresses: nam-trung.nguyen@griffith.edu.au (N.-T. Nguyen), hongjie.an@griffith.edu.au (H. An).

https://doi.org/10.1016/j.molliq.2025.126873
Received 6 October 2024; Received in revised form 18 December 2024; Accepted 6 January 2025
Available online 12 January 2025
0167-7322/

such methods can control the generation of specific types of gas nanobubbles[19] and provide stable control over nanobubble size [12,20] and concentration [21,22], the energy requirements and operational costs associated with these methods are still high.

The structure of the solid surface is crucial for the pinning of surface nanobubbles and plays a significant role in the spontaneous formation of surface nanobubbles, particularly at hydrophobic interfaces [23–25]. Agrawal et al. [26] and Bao et al. [27] found that nanobubbles nucleated primarily in hydrophobic regions. Wang et al. [28] observed nanobubble formation on the hydrophobic region on the surfaces covered with nanopores. The nucleation mechanism on those hydrophobic surfaces was later explained using a two-step theory [17]. Using porous materials with different hydrophobicity presents a promising and energy-efficient strategy for spontaneous, cost-effective, and reproducible bubble generation without significant energy input.

In this paper, we experimentally demonstrate that bubble suspensions of tuneable composition can be created with almost no energy simply through careful choice of materials. Microporous materials such as metal–organic frameworks, active carbon and molecular sieves are frequently used in ambient conditions for applications such as gas capture, purification and drying [29–32]. These materials have a strong native affinity for gases, thus removing them from the ambient environment [33]. Carbon molecular sieves (CMS) are often used in pressure swing adsorption (PSA) techniques to generate pure nitrogen or oxygen [34]. Whereas Zeolite 4 Å molecular sieves (ZMS) have been reported to possess the ability for nitrogen adsorption and, therefore, concentrate oxygen [35,36]. When those microporous materials are deployed in liquids, they may serve as gas sinks, releasing gas into surrounding liquids and significantly raising the dissolved gas concentrations. This increased dissolved gas saturation further facilitates the nucleation of large quantities of bubbles without the need to agitate the liquid or apply electrical currents mechanically. In this paper, we will systematically demonstrate how to generate micro/nanobubbles with these microporous materials. We will also demonstrate that this method of producing bubble suspensions is even capable of gas selectivity, with zeolite molecular sieves producing nitrogen-rich liquids and carbon molecular sieves producing oxygen-rich liquids.

2. Materials and methods

2.1. Materials

The CMS was purchased from Kuraray Co., Ltd, with a pellet diameter of 1.4–1.6 mm and a bulk density of 0.65–0.70 g/ml [37]. ZMS in the form of small beads of 1.6–2.5 mm and a bulk density of 0.7–0.8 g/ml were purchased from Aus Chem Source Pty. Ltd. Milli-Q water was from Milli-Q® Direct Water Purification System with a conductivity of 18.2 MΩ. Surfactants, sodium dodecyl sulphate (SDS, ≥99 %) and Cetyltrimethylammonium bromide (CTAB, ≥99 %) were purchased from Sigma-Aldrich, and Tween 20 (T20, ≥99 %) and Sodium sulphite (≥99 %) were purchased from ChemSupply, Australia. All chemicals were used as received (with analytical grade or better) without further purification.

2.2. Nanobubble generation

The molecular sieves were cleaned before use. They were first rinsed with ethanol, then vacuum dried for 5 h at 200 °C, followed by rinsing with Milli-Q water and vacuum drying at 200 °C. The cleaning process was repeated three times. The cleaned molecular sieves were immersed in Milli-Q water or surfactant solutions, Fig. 1. The stock surfactant solutions were prepared based on critical micelle concentration (CMC) of SDS, T20, and CTAB of 8.2 mM, 0.06 mM, and 0.92 mM, respectively. The solutions were diluted with Milli-Q water and filtered with a 20-nm membrane before use. To generate nanobubbles, a volume of 40 ml solutions at a given concentration of SDS, T20 and CTAB was added into

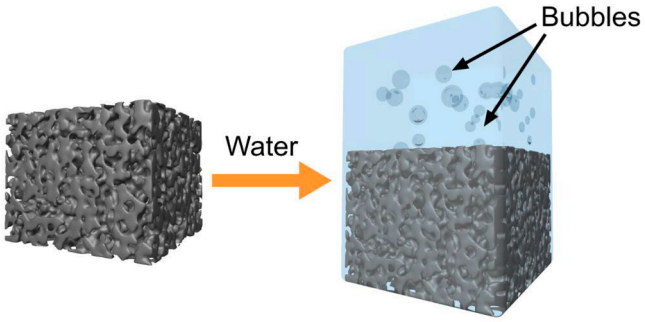

Fig. 1. Schematics of CMS bubble solution collection.

20 g cleaned dry CMS samples. The solutions were gently added along the wall of the container to flow into the CMS, avoiding entrapping gas bubbles. Subsequently, the system was held still for 20 min. Some samples were collected for characterisation, and others were subjected to degassing.

2.3. Degassing

Degassing was carried out by a protocol called freeze–pump–thaw under a vacuum. This degassing treatment was reported as an effective method for solution degassing [2,7]. The water samples were poured into a flask, vacuumed and frozen with external liquid nitrogen. After freezing, liquid nitrogen was removed, and the system was kept under a vacuum while the solutions thawed to room temperature. The degassing process was repeated three times.

2.4. Characterisation

The molecular sieve-treated solutions were characterised by a Nanoparticle Tracking Analysis (NTA) system (Nanosight NS300, Malvern Panalytical) and Dynamic Light Scattering (DLS) instrument (LiteSizer 500, Anton Paar). The zeta potential was measured with LiteSizer 500. Dissolved oxygen (DO) level was measured with a commercial oxygen meter (Smart Sensor AR8406, GRAIGAR). The oxygen meter probe was calibrated for a zero-point oxygen concentration using sodium sulphite solutions before use. The scanning electronic microscope (SEM) cross-section images of the CMS and ZMS pellet were acquired by a JEOL JSM 7100F SEM system. The CMS and ZMS samples for cross-section SEM were prepared by cutting at the middle of each pellet and sticking them on the 90-degree SEM specimen mounts with conductive double-sided carbon tape. A Biolin Scientific Theta Flex optical tensiometer was used to measure the contact angle.

3. Results and discussion

3.1. Structures of CMS and ZMS

The fine structures of the molecular sieves were analysed by SEM. Fig. 2 shows the cross-sections of CMS and ZMS, displaying the porous structure of the materials. Fig. 2A and C show that both CMS and ZMS exhibit densely distributed micrometre-scale pores (macroporous). Upon closer examination of the magnified images, the macroporous of CMS exhibits a size of 1.77 ± 0.52 μm, while those in ZMS are 0.54 ± 0.21 μm. This clearly indicates that the pore sizes in CMS are significantly larger than those in ZMS. One notes that both CMS and ZMS have nominal pores of 4 Å, much smaller than the resolution of the SEM characterisation method. Therefore, the macropores observed in the SEM images are not molecular-level pores, but rather the “large” cracks or crevices between the microparticles in the molecular sieves’ structure.

As shown in Fig. 2B, the cross-sectional view of CMS presents a

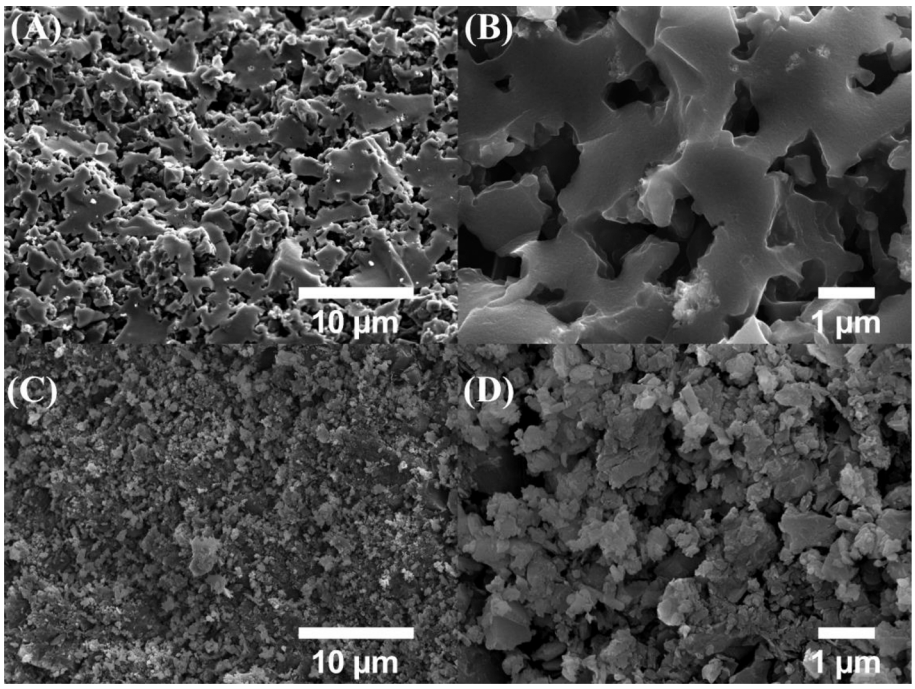

Fig. 2. Cross-section images of carbon molecular sieve (A, B) and zeolite molecular sieve (C, D) using SEM. The scale bar in (A) and (C) is 10 μm, and 1 μm in (B) and (D). The magnification in (A) and (C) is ×1,000, and ×15,000 in (B) and (D).

relatively uniform structure, indicating that its internal surface resembles the structure found on graphite basal planes. In contrast, the cross-section of ZMS is quite rough, likely due to the sintering processes during fabrication. These processes caused the microporous structure with a pore size of 0.54 ± 0.21 μm, derived from grain boundaries. The micropore structure of ZMS is attributed to its unique SiO_4 and AlO_4

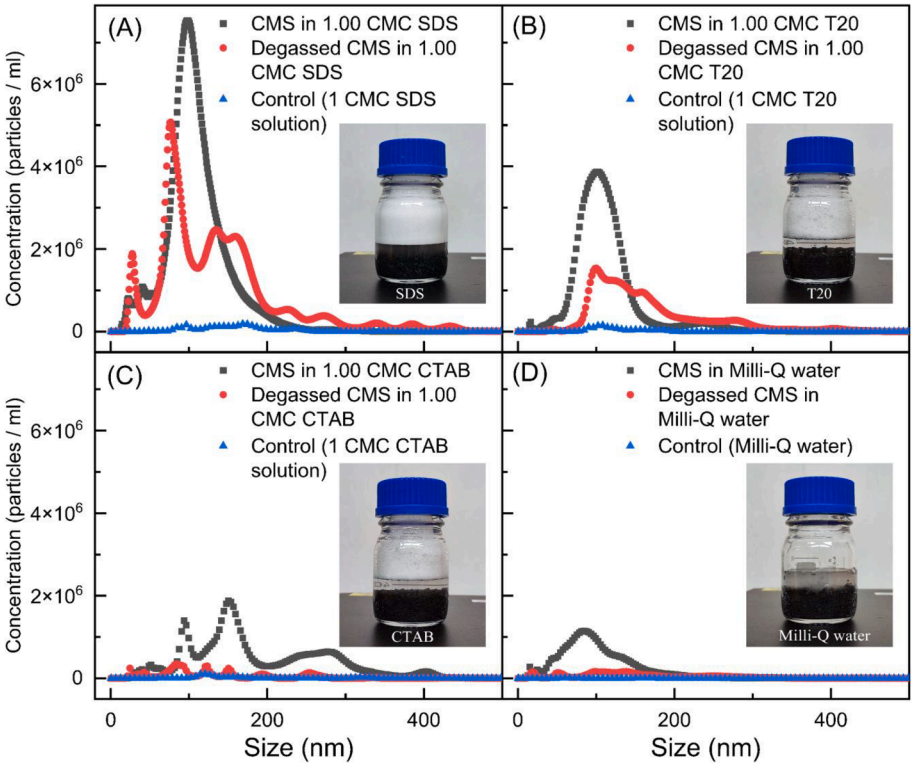

Fig. 3. Size distribution and concentration of nanoparticles by NTA collected from (A) CMS in 1-CMC SDS solution, (B) CMS in 1-CMC T20 solution, (C) CMS in 1-CMC CTAB solution, (D) CMS in Milli-Q water (black solid cube) and their corresponding degassed samples (red solid). The blue triangles represent the control group data acquired from pure Milli-Q water without adding CMS. The inset image represents the CMS after adding 40 ml SDS solution, T20 solution, CTAB solution (at a concentration of 1 CMC), and Milli-Q water, respectively. The images of CMS with solutions are all captured below 30 s after adding solutions. (For interpretation of the references to colour in this figure legend, the reader is referred to the web version of this article.)

tetrahedral configurations [38].

3.2. Bubbly water

Milli-Q water and other solutions are slowly added along the sidewall into the vial containing the CMS or ZMS since we do not intend to introduce any gas that can entrap bubbles in solutions [11,18]. Once the solutions were in place, we recorded the reactions. Instant bubbling was observed upon exposure of the solutions to CMS, as indicated in the insets of Figs. 3 and S1. We observed rapid and continuous gas release when CMS was exposed to water, and the resulting dissolved gas oversaturation led to bubbling and foaming in the solutions [39]. Macro bubbles float up by buoyancy to leave the system and burst at the air/water interface under the gas oversaturation. The same phenomenon also occurred in ZMS solutions, as shown in Fig. S2. However, the ZMS sample did not give rise to bubbles as much as the CMS samples. For a careful experiment, we used Milli-Q water and different surfactants at a concentration of 1 CMC. Foams formed in both molecular sieves samples when the molecular sieves were immersed in surfactant solutions and showed a foggy and milky white colour. The foam did not pop but expanded into the air phase. Foams formed vigorously in all surfactant solutions, and the reaction proceeded to be particularly severe in SDS solutions. After 20 min, the foam overflowed in all solutions that contained surfactants. SDS solutions generated the most foam, followed by T20, while CTAB solutions produced the least amount. The remaining solutions were slightly turbid in SDS because of the large amounts of bubbles released. However, they are relatively clear in the cases of T20 and CTAB. No foams were observed in the Milli-Q water group, which appeared as milky emulsion-like bubbly water, indicating that bubbles remain in the liquid phase. We then passed a green laser beam through the remaining solutions, Fig. S3. All sample solutions show a highly noticeable green line path, the resulting scattered light in the presence of nanoscale particles known as the Tyndall effect. In comparison, all control solutions, Milli-Q water and surfactant solutions, except for CTAB before introducing CMS, show no visible green laser line. Similar results were also obtained with ZMS samples, Fig. S4. As these solutions were filtered by a 20-nm membrane, some particles were possibly removed. The CTAB control solutions show a relatively weak green line for unknown reasons. The light intensity is much weaker than the CTAB solutions after CMS treatment, so it could be ignored. Fig. S1 and the insets of Fig. S2 indicate that introducing different solutions into porous materials, such as CMS and ZMS, can trigger the release of a substantial amount of gas stored within the interstices of these materials into the solution. The above result confirmed our hypothesis. This phenomenon leads to a significant increase in gas oversaturation within the solution, thereby resulting in the formation and enrichment of nanobubbles. We then characterised the remaining water solutions to test the nucleation and stability of nanobubbles.

3.3. Characterisation of bubbly water

To obtain the size and concentration of the resultant solution, we characterised all four samples using NTA and DLS. Fig. 3 shows the concentration and size distribution of CMS within 1 CMC SDS, T20, CTAB solution and Milli-Q water. The control group, without adding to CMS, gave rise to negligible particle concentrations, indicating a clean environment. This is consistent with the laser scattering tests, as shown in Fig. S3.

Fig. 3 shows that all CMS-treated solutions have particles in a range of 200 nm centred around approximately 100 nm. The peak concentration in SDS, T20, CTAB and Milli-Q water are 7.5×10^6, 3.9×10^6, 1.9×10^6, and 1.1×10^6 particles/ml, respectively, meaning the concentration of particles gradually decreases in a sequence SDS > T20 > CTAB > Milli-Q water (Fig. 3). The total concentrations are 4.7×10^8 particles/ml for SDS solutions, 2.6×10^8 particles/ml for T20 solutions, 1.9×10^8 particles/ml for CTAB solutions, Milli-Q water: 1.0×10^6 particles/ml for Milli-Q water as shown in Fig. 4 (B). The discrepancy here suggests that the type of surfactants significantly influence the generation and stability of nanoscale particles. The size distribution in the CTAB sample displays multiple peaks, which is different from the other three samples. The mode size of the other three samples was recorded as 97 nm, 100 nm, and 87 nm in SDS, T20, and Milli-Q water, respectively. The data of CTAB indicates poor polydispersity and maybe also poor stability of colloidal solutions. The introduction of surfactants also effectively facilitates both the concentration and stability of nanoscale particles in the ZMS solution. ZMS with SDS solution also exhibits higher peak intensity and integral concentration, Fig. S5.

To elucidate the performance of observation of concentration in different solutions. We measured the zeta potential of each sample, as shown in Fig. 4C. In all tested samples, the zeta potential consistently exhibited absolute values in the range of dozens of millivolts, signifying the relatively stable preservation of nanobubbles. This contrasts with the zeta potential value of approximately 0 mV obtained in Milli-Q water. Notably, the SDS solution, featuring negatively charged hydrophilic groups, showed a zeta potential value of -50 ± 4 mV, while CTAB, with

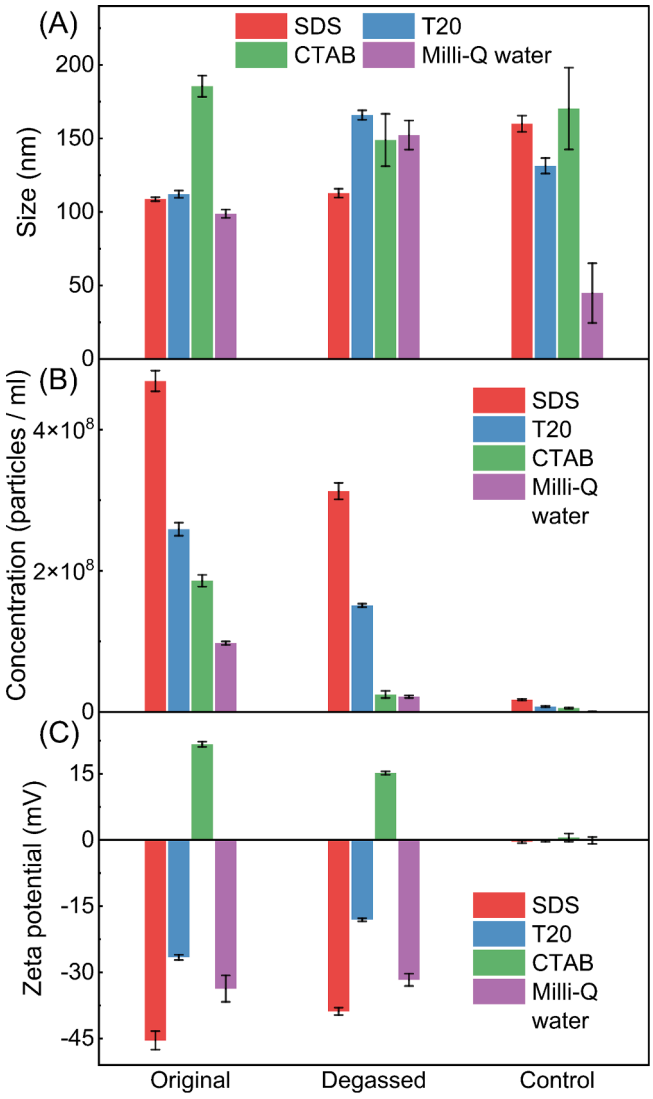

Fig. 4. The size (A) acquired and total concentration (B) of the nanoparticles obtained from NTA, the zeta potential (C) obtained from the DLS of different CMS BNBs solutions of CMS in 1CMC SDS solution, T20 solution, CTAB solution, and Milli-Q water. The original group represents the CMS-treated solutions before degassing, and the control group stands for the stock solutions with no CMS addition.

positively charged hydrophilic groups, displayed a value of around 22 ± 5 mV. Furthermore, the electro-neutral T20 solution (−27 ± 3 mV) and the non-charged Milli-Q water solution (−34 ± 10 mV) both exhibited negative zeta potential values. In all four solutions, nanoparticles in CTAB were positively charged, while the other three had negative charges. So, we inferred that the poor stability of particles in CTAB results from the surface charges.

These observations agree with the longstanding understanding of the presence of a negative charge at gas–liquid interfaces. It implies that the introduction of CMS, even in non-ionic solutions, leads to a sustaining stable gas–liquid interface, additionally, according to Tan et al. [24,40], the surface charge density of BNBs is the key to their stability, providing electrostatic stress on the surface and acting radially outward. The repulsion between charges cancels the Laplace pressure arising from the surface tension of the gas–liquid interface, providing a stable pressure balance between the inside and outside of a BNB. The negative zeta potential values in SDS, T20, and Milli-Q water solutions suggest that the nanoscale particles in the solution are highly likely to be nanoscale gas entities. Moreover, following the principles of colloidal solutions, higher absolute values of zeta potential in the solution indicate a more stable colloidal particle dispersion. Therefore, the nanobubbles in SDS solutions exhibited a relatively uniform size distribution and a higher concentration compared to the other three groups. In CTAB solutions, however, the positively charged hydrophilic groups carried by surfactant molecules at the gas–liquid interface cancelled out some of the accumulated negative charge, resulting in a relatively unstable colloidal system as well as a low number of positive surface charge densities (Fig. 4C). This finding agrees with the irregular size concentration distribution of gas nanoscale entities depicted in Fig. 3.

3.4. Proof of gas by degassing of bubbly water

The use of NTA is limited by the ability not being able to distinguish the nanoparticles, nanobubbles, and nanodroplets [41]. Other characterisation methods are required to identify further if the nanophase entities are bubbles, droplets, or particles. Degassing is employed in this experiment. If these nanophases contain gases, further NTA measurement will observe a reduction in the amount or clearance of the nanophases. In contrast, if the nanophases are nanoparticles, the degassing would not influence their concentration with unchanged size.

The concentration peak of the CMS SDS sample is 7.6×10^6 particles/ml (Fig. 3A), which is reduced to 5.1×10^6 particles/ml after degassing. The peak concentration of the T20, CTAB, and Milli-Q water samples all show a significant drop after degassing (Fig. 3B-3D). This suggests that the degassing process removes a considerable number of nanoparticles. In addition, based on the total concentration obtained from Fig. 4 (B), in the case of CTAB and Milli-Q water, we saw the degassing basically removed all the generated “nanoparticles”, which could be attributed to gas nanobubbles. At the same time, in surfactant samples, a proportion of nanobubbles remained after degassing. This could be micelles of surfactant themselves encapsulating the bubbles. Degassing could cause a collapse of bubbles and a coalescence of surfactant skins, so the remaining bubbles integrate into larger ones. This is evidenced by the broadening of size after degassing, as shown in Fig. 3. It could also be possible if some nanobubbles leached out from molecular sieve materials with the assistance of surfactant.

The degassing process reduces the gas solubility in the solution, causing gas to precipitate into the existing BNBs and significantly increasing their sizes, which can be observed in T20 and the Milli-Q water samples. However, although the total concentration dropped to half of the original specimen in the SDS sample, the mean size did not change too much. At the same time, we can also notice that the size distribution of the degassed SDS sample tends to be bimodal. Under reduced pressure, gas dissolved within the solution is also reduced due to Henry’s law; degassing by reduced pressure actually causes oversaturation under that reduced pressure, which causes the aqueous gas to change into gaseous gas. We usually observe gas growing in the early phase of vacuum until it rises up and leaves the liquids. This is the reason for the wider, larger peak observed in the degassed sample. At the same time, the solubility increases when the gas pressure returns to normal. The reduced gaseous gas during the depressurisation progress causes the undersaturation of the solution, leading to the dissolution of gas from the nanobubbles into the solution and resulting in a reduction in bubble size. Due to the presence of surfactants, both the large-sized nanobubbles generated during the depressurisation phase and the small-sized nanobubbles generated during the undersaturated phase can reach an equilibrium state.

3.5. Effect of surfactant

The influences of the concentration of surfactant on size and concentration were investigated to determine whether the results interfered with micelle formation. Fig. 5 shows the concentration of surfactant determined concentration versus size distribution, mean size, total concentration, and zeta potential of BNBs solution in SDS with different CMC ratios (0.25, 0.5, 0.75, 1, 1.5, 2) and CMS in Milli-Q water solution, alone with the pure Milli-Q water as the control group. Fig. 5A shows that almost all SDS samples exhibit higher concentration peaks than Milli-Q water. Whether at 0.25 CMC or 2 CMC, the maximum peak concentration is distributed at around 6×10^6 particles/ml, and the samples at 0.5 CMC and 1.0 CMC show peak intensities close to 8×10^6 particles/ml. Fig. 5(B) clearly shows that the size of BNBs gradually decreases with the increasing concentration of the surfactant, reducing from approximately 120 nm to around 100 nm. However, the concentration counts of BNBs show similar values among these samples, with only a slight difference in the 0.25 CMC sample. Meanwhile, the zeta potential of these samples increases gradually with the surfactant concentration. Furthermore, we conducted tests for T20 and CTAB with different CMC ratios to study the size and concentration changes, as shown in Figs. S6 and S7. The T20 solution exhibits a similar trend to the SDS solution. However, the size distribution of BNBs in the CTAB solution does not show a single peak, as seen in SDS and T20. Instead, multiple peaks with low intensities were observed. This may be related to the accumulation of positive charges at the gas–liquid interface caused by the cationic surfactant CTAB solution.

3.6. Stability of nanobubbles

Fig. 6 depicts the overnight dynamic changes of CMS and ZMS-derived nanobubbles from CMS solutions containing SDS and Milli-Q water. It is evident that nanobubbles exist in all these solutions for at least 7 days, even if they have exhibited relatively variable scattering intensity and bubble size. However, the fluctuation in size and intensity manifests the observed nanoscale entities as gaseous nanobubbles, as nanoparticles would not change in size during long-term measurement. In the CMS BNBs solution, the intensity of light scattering peaks mainly centred around 200 nm, with an obvious difference in the two solvents. These sizes show minimal variation in diameter over the 24 h of nanobubble generation. In contrast, the intensity distribution of light scattering for ZMS BNBs solution displays relatively irregular fluctuations, indicating the complex size distribution variations over time. However, after 6 h, the size distribution tended to be stable and moved towards smaller size for both SDS and Milli-Q samples. This may imply that the “big” bubbles generated through the gas oversaturation either ruptured at the surface by the buoyancy or burst to form smaller gas bubbles.

To evaluate the stability of nanobubbles, we also monitored the concentration of various nanobubble solutions over 7 days, with the results presented in Supplementary Figs. S11–S16. These data suggest that while the concentration of nanobubbles gradually decreased, they remained relatively stable over the 7-day period. Good stability was observed with Milli-Q water (Figs. S14 and S16) and with the surfactant SDS (Figs. S12 and S15). However, In CTAB solutions, nanobubble

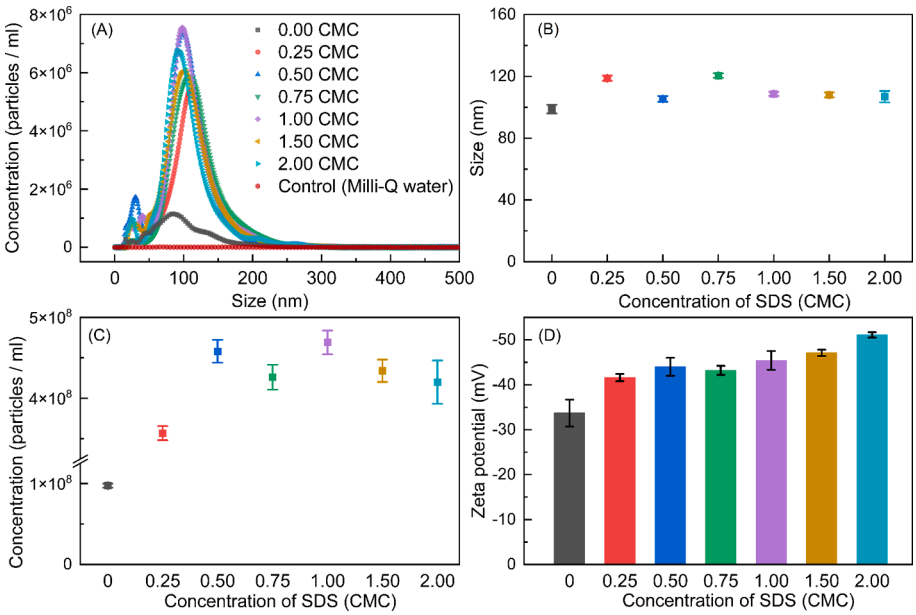

Fig. 5. Nanoparticle tracking analysis (NTA) size distribution curves of nanobubbles collected from (A) CMS in different ratios of CMC SDS solution. The mean size of each CMC solution acquired from NTA and the total concentration of the nanoparticles is shown in (B) and (C), respectively. The zeta potential is shown in (D).

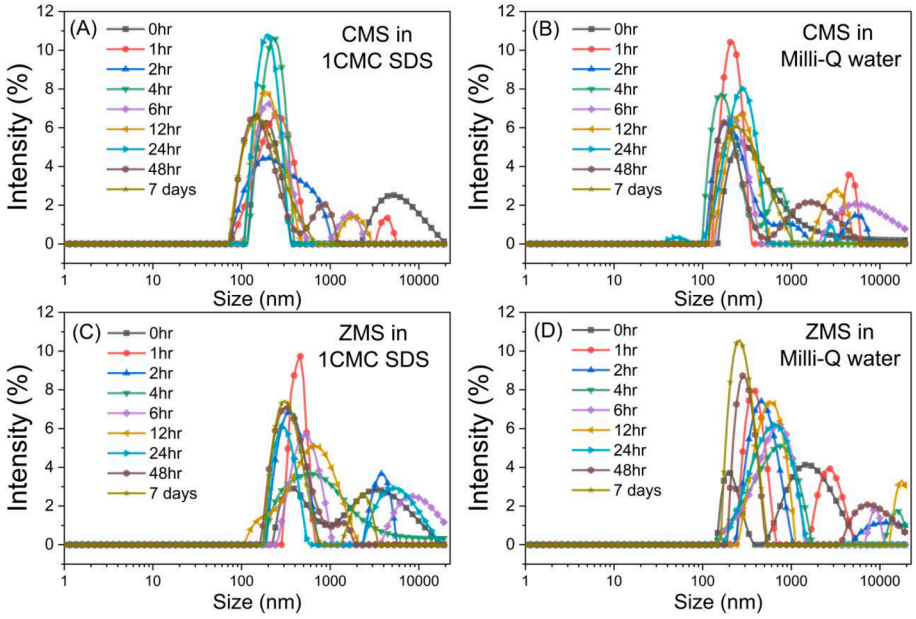

Fig. 6. Long-term stability of BNB solutions. (A) CMS-treated 1CMC SDS solution, (B) CMS-treated Milli-Q water, (C) ZMS-treated 1CMC SDS solution, and (D) ZMS-treated Milli-Q water.

concentration dropped to about half before reaching an equilibrium. Nanobubbles in the T20 solution (Fig. S13) show a similar trend to that observed in the CTAB solution. Interestingly, the average size of nanobubbles did not change significantly.

3.7. Gas saturation of bubbly water

Since the adsorption rate of oxygen in CMS is way higher than that of nitrogen [42], we hypothesised that CMS-treated water would end up oversaturating DO by releasing the adsorbed oxygen into the water. Then, we measured the DO in the resultant solutions over time. Fig. 7A shows that in atmospheric conditions, when immersing CMS in water, the DO reduced with time, starting from 8 ppm and finally dropping and staying stable at 5 ppm. This observation is opposite to our prediction. Further, in the case of pressure changes, the DO dropped to ~3 ppm and 3.5 ppm at equilibrium. In contrast, for nitrogen adsorption, preferred ZMS [33,43], we expected an oversaturation of dissolved nitrogen. In fact, the DO meter reading shows the DO has risen to 11 ppm under ambient pressure and 12 ppm under pressure changes and equilibrated at 10 ppm and 11.5 ppm, respectively. We calculated the oversaturation of the solutions by using the equation

$$\zeta = \frac{c - c_s}{c_s} \tag{3.1}$$

where c is the concentration of DO, which can be measured by a DO metre and c_s is the solubility of oxygen in water. CMS-treated water has a

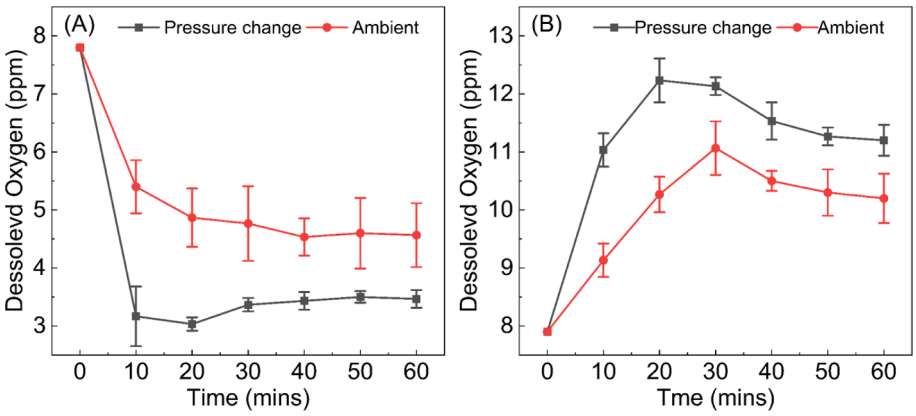

Fig. 7. Dissolved oxygen level versus time of different original solutions (first column) and the corresponding (A) CMS and (B) ZMS BNBs solutions. The black cube represents the measured CMS or ZMS experienced vacuum first for 10 mins and then air pressured at 3 atm for another 10 min; the red circle is for the CMS or ZMS measured in ambient. The dissolved oxygen concentration at t = 0 mins represents the saturated oxygen level in each case, which is 7.8 for CMS measurement and 7.9 for ZMS measurement, respectively. (For interpretation of the references to colour in this figure legend, the reader is referred to the web version of this article.)

DO of ~4.6 ppm in an ambient environment and 3.5 ppm after pressurised air treatment with corresponding calculated oversaturation levels of −0.41 and −0.56, respectively. This is referred to as the undersaturation of DO in the CMS-treated solution. This undersaturation of DO means that the nanobubbles in CMS-treated water are not oxygen nanobubbles since the oxygen might dissolve rapidly due to diffusion theory if they are oxygen nanobubbles. For water treated with ZMS, we observed a DO concentration of approximately 11 ppm in the absence of pressure changes and 12 ppm when pressure changes were introduced. This resulted in oversaturation levels of 0.38 and 0.5, respectively. It is important to note that both instances indicate the presence of oxygen nanobubbles within the ZMS-treated water. Meanwhile, the ZMS has the capability to adsorb nitrogen, which contradicts our DO meter readings and shows oversaturation of oxygen.

Our data strongly suggests that the removal of dissolved nitrogen can lead to an increase in the oversaturation of DO. This phenomenon bears a resemblance to the findings of Yamashita and Ando [44], who reported that by bubbling purge nitrogen gas into water, a saturated solution can be transformed into one that is oxygen-unsaturated but oversaturated with dissolved nitrogen. Conversely, the oversaturation of DO can result in undersaturation of dissolved nitrogen. Yamashita's study implies the existence of an interplay between these two gaseous components dissolved in water, where an increase in the concentration of one gas leads to a decrease in the concentration of the other. In our own observations, when we introduced CMS and ZMS into the water, we noticed a bubbling effect. In line with Yamashita's findings, bubbling nitrogen gas into the water reduced the DO levels. When CMS treatment induced bubbling and correspondingly decreased DO levels, it suggests that CMS may be responsible for the release of nitrogen gas through bubbling. Conversely, ZMS treatment also led to bubbling but with increased DO levels, implying that oxygen was being introduced through bubbling in this case. In our experiment, once water is introduced, the gas captured in the macropores of CMS, which consist of a considerable amount in CMS [42], will dissolve into water. The gas assembled in the macropores is mostly nitrogen, which has been repelled by oxygen molecules occupied in the sub-nano micropores. In other words, water gradually permeates to macropores (~1.8 μm, Fig. 2), which may further lead to the displacement of nitrogen by water. The surface of 'old' graphite, exposed to ambient conditions for several hours, has a characteristic contact angle of ~60° [45], which may be because of the formation of hydrogen bonds between water and oxide species [46], suggesting partial hydrophilic wetting, which contributes to water penetrating in CMS. We have also implemented the contact angle measurement of CMS, as shown in Fig. S18; the contact angle of water droplets on the CMS surface is exhibited within the range of ~60° to 70°, corresponding to the reported contact angle of this specific material. These factors cause bubbling once CMS is immersed in water. Therefore, dissolved nitrogen builds up in solutions with CMS.

Our experimental results deviate from our initial expectations. In order to ascertain whether the observed changes in DO levels were solely attributable to the bubbling process, we decanted the equilibrated bubbly water and replaced it with fresh Milli-Q water in the presence of CMS and ZMS. Remarkably, the same patterns persisted: CMS induced a decrease in DO levels, while ZMS led to an increase in DO levels in DI water. These findings indicate another reason for the paradox of the DO change in those molecular sieves: CMS continues to adsorb DO, while ZMS predominantly adsorbs dissolved nitrogen.

A decrease in DO indicates CMS continuing to adsorb oxygen dissolved in water. This is supported by previous studies that carbon surfaces exhibit a relatively strong affinity for oxygen gas molecules at room temperature due to the formation of specific types of carbon–oxygen surface complexes [47]. This is supported by the Langmuir fitting results that CMS has a relatively high surface area of 640.9 m^2/g and higher adsorption capacity for pure oxygen (3.27 mol kg^{-1}) compared to pure nitrogen (2.44 mol kg^{-1}) at 1 MPa [42]. These gas phase studies may apply to the adsorption of dissolved gas, according to a recent study conducted by Petsev et al. [48] and Tan et al. [49], who have suggested that those carbon pores have high adsorption enthalpy of dissolved gases in water. The fact that CMS will continue to adsorb oxygen could result in less oxygen content in water.

The DO dropped to approximately 65 % under pressure changes applied to CMS, which can be attributed to a series of intricate mechanisms. The initial reduced pressure treatment of CMS effectively evacuates adsorbed gases, including oxygen, nitrogen, and water vapour, thereby creating additional unoccupied binding sites conducive to further oxygen adsorption. However, some sites within the CMS structure may remain occupied by water vapour molecules, particularly at the "bottle-neck" regions of the micropores and on the oxide species present on the carbon surface due to hydrogen bonding interactions [46,50]. Subsequent exposure to pressurised air increases oxygen adsorption, resulting in the retention of more nitrogen within the macropores of the CMS. When water permeates these materials, nitrogen is released into the solution, causing a reduction in DO levels. This highlights the complex dynamics of gas adsorption and release within the CMS structure under varying pressure conditions.

Furthermore, we purged the CMS with pure nitrogen and oxygen gas (Fig. S9). These treatments significantly increased the nanobubble concentration in the solution. The treatment with pressured nitrogen resulted in a lower level of DO compared to the ambient one but similar to the air-pressured treatment, indicating the fact that the nanobubble

mainly consists of nitrogen. In contrast, the oxygen-treated experiment exhibited a high DO level, suggesting the generation of oxygen nanobubbles.

In the case of ZMS, we observed a gentle bubbling effect and a simultaneous increase in DO levels for both scenarios, with and without pressure changes. The subdued bubbling observed with ZMS may be attributed to the relatively smaller size of their macropore (approximately 0.5 μm) and the accessibility of these pores (Fig. 2a, SEM image). The observed elevation in DO levels when using ZMS, whether they were pre-treated with or without pressure changes, can be attributed to a dual mechanism. Similar to CMS, ZMS may facilitate DO increase by both actively promoting bubbling and continuously adsorbing dissolved nitrogen. Notably, the increase in DO levels was also evident when bubbly water was replaced with fresh water, suggesting that ZMS possesses the capacity to adsorb dissolved nitrogen, thereby attracting more air to dissolve in the water. Similar to the CMS, in the pure oxygen and nitrogen purging-treated ZMS samples, the total nanobubbles concentration increased after purging. The DO level dropped with the pure nitrogen-treated ZMS, Fig. S10, suggesting nitrogen nanobubbles. However, pure oxygen-treated ZMS shows a high DO level, indicating the oxygen nanobubble generated by the ZMS.

3.8. Verification of gas type in nanobubbles

To further confirm the type of gas in the produced nanobubbles, we added an excessive oxygen scavenger (sodium sulphite) to remove the dissolved oxygen from the solutions and characterised the size distribution before and after the oxygen scavenger treatment (Figs. 8 and S8). Here, we use Milli-Q water to generate nanobubbles in solution to minimise the impact from surfactants. It clearly shows that the sodium sulphite does not change the concentration of nanobubbles in the solution treated by CMS. Despite a slight reduction in peak concentration, the overall size distribution remains stable. In contrast, the addition of an oxygen scavenger to ZMS-treated water has resulted in a significant drop in concentration. The peak concentration reduced to approximately one-third of the initial level, and the total concentration also dropped from 10.6×10^8 particles/ml to 5.5×10^7 particles/ml (Fig. S8). The size was not affected compared to before and after the oxygen removal. We also found similar results in the 1CMC SDS solution, as shown in Fig. S17. These results suggest that most of the 'nanoparticles' produced by ZMS were primarily filled with oxygen. This experiment supports our findings in Fig. 7.

When immersing porous materials in water, the adsorbed gases in the pores are gradually released, resulting in an oversaturation of dissolved gas. With more and more gas molecules dissolved into bulk water, bubbles nucleated and stabilised, possibly by some contaminations, e.g., some unproven additives from molecular sieves. No matter what species of oversaturation, both offer potential applications for molecular sieve materials in various scenarios. For instance, controlling the oxygen concentration in wastewater treatment by adding ZMS can enhance the dissolution of pollutants in water [51]. In anaerobic fermentation processes, incorporating CMS can boost fermentation yields, among other potential applications [52]. In addition, all the molecular sieves used in this experiment can be reactivated for recycling, which is environmentally friendly and sustainable.

This work was conducted with an open water system, and the main findings are that the oversaturation of DO and undersaturation can be formed using specific porous materials, which can guide their further use. These are exciting topics and worth working on in the near future. It may also come to some interesting results if we use the compound of the two molecular sieves of ZMS and CMS with different ratios. These studies are attracting interest in specific fields, particularly biomedical engineering. The findings in this paper are not just limited to ZMS and CMS; other porous materials with similar capabilities of capturing specific gases can perform similarly.

4. Conclusions

In summary, we present an efficient method for producing suspensions of fine bubbles suspensions with low energy cost, addressing two key technological challenges in the fine bubble industry. Our method exploits the strong gas affinity of commercial gas capture materials, carbon molecular sieves (CMS) and zeolite molecular sieves (ZMS), to absorb specific gases from the ambient atmosphere and create a gas-enriched liquid environment. The choice of microporous material allows for control over the gas composition of the resulting bubble suspensions, with high or low dissolved oxygen values for various applications. Surfactants play a role in nanobubble generation and stability, with SDS solutions yielding the highest concentration and stability. These nanobubble suspensions demonstrated remarkable stability, persisting for at least 24 h. Our results pave the way for industrial applications of ultrafine bubble technologies to reach their full potential in various fields, including aquaculture, wastewater treatment and biotechnology.

CRediT authorship contribution statement

Lingxi Ouyang: Writing – review & editing, Writing – original draft, Visualization, Methodology, Investigation, Formal analysis, Data curation. **Haotian Cha:** Writing – review & editing. **Jun Zhang:** Writing – review & editing. **Helena H.W.B. Hansen:** Writing – review & editing, Visualization. **Qin Li:** Writing – review & editing. **Beng Hau Tan:**

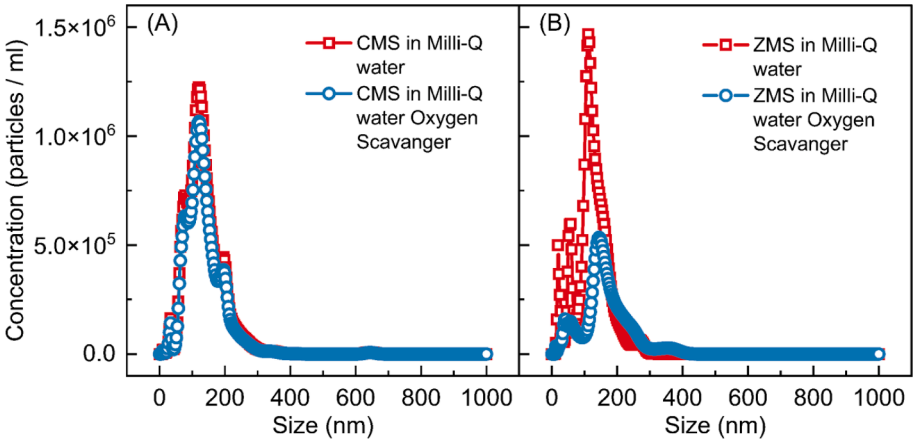

Fig. 8. Size distribution of BNBs water solution in (A) CMS and (B) ZMS before and after the oxygen removal. The significant drop in concentration of nanobubbles in (B) with oxygen scavenger in ZMS treated solution indicates that ZMS create an oxygen-rich environment, while CMS does not.

Writing – review & editing. **Porun Liu:** Writing – review & editing. **Dongke Zhang:** Writing – review & editing. **Liang Wang:** Writing – review & editing, Formal analysis. **Nam-Trung Nguyen:** Writing – review & editing. **Hongjie An:** Writing – review & editing, Supervision, Project administration, Methodology, Conceptualization.

Declaration of competing interest

The authors declare that they have no known competing financial interests or personal relationships that could have appeared to influence the work reported in this paper.

Acknowledgements

H.A. acknowledges the support from the Australian Research Council Future Fellowship (FT180100361) and Discovery Project (DP230100556).

Appendix A. Supplementary material

Supplementary data to this article can be found online at https://doi.org/10.1016/j.molliq.2025.126873.

Data availability

Data will be made available on request.

References

[1] N.J. English, Sustainable exploitation and commercialization of ultradense nanobubbles: reinventing liquidity, ACS Sustain. Chem. Eng. 10 (2022) 3383–3386, https://doi.org/10.1021/acssuschemeng.2c01058.
[2] J. Zhu, H. An, M. Alheshibri, L. Liu, P.M.J. Terpstra, G. Liu, V.S.J. Craig, Cleaning with bulk nanobubbles, Langmuir 32 (2016) 11203–11211, https://doi.org/10.1021/acs.langmuir.6b01004.
[3] H.H.W.B. Hansen, L. Ouyang, H. Cha, J. Zhang, Q. Li, B.H. Tan, A. Vashi, N.-T. Nguyen, H. An, Surface cleaning of oil contaminants using bulk nanobubbles, ChemSusChem (2024) e202400802, https://doi.org/10.1002/cssc.202400802.
[4] S. Waters, D. Hamilton, G. Pan, S. Michener, S. Ogilvie, Oxygen nanobubbles for lake restoration—where are we at? A review of a new-generation approach to managing lake eutrophication, Water 14 (2022) 1989.
[5] A.W. Foudas, R.I. Kosheleva, E.P. Favvas, M. Kostoglou, A.C. Mitropoulos, G. Z. Kyzas, Fundamentals and applications of nanobubbles: a review, Chem. Eng. Res. Des. 189 (2023) 64–86, https://doi.org/10.1016/j.cherd.2022.11.013.
[6] H.H. Hansen, H. Cha, L. Ouyang, J. Zhang, B. Jin, H. Stratton, N.-T. Nguyen, H. An, Nanobubble technologies: applications in therapy from molecular to cellular level, Biotechnol. Adv. (2022) 108091.
[7] J. Qiu, Z. Zou, S. Wang, X. Wang, L. Wang, Y. Dong, H. Zhao, L. Zhang, J. Hu, Formation and stability of bulk nanobubbles generated by ethanol–water exchange, ChemPhysChem 18 (2017) 1345–1350, https://doi.org/10.1002/cphc.201700010.
[8] J. Wu, K. Zhang, C. Cen, X. Wu, R. Mao, Y. Zheng, Role of bulk nanobubbles in removing organic pollutants in wastewater treatment, AMB Express 11 (2021) 96, https://doi.org/10.1186/s13568-021-01254-0.
[9] L.-M. Zhou, S. Wang, J. Qiu, L. Wang, X.-Y. Wang, B. Li, L.-J. Zhang, J. Hu, Interfacial nanobubbles produced by long-time preserved cold water*, Chin. Phys. B 26 (2017) 106803 https://doi.org/10.1088/1674-1056/26/10/106803.
[10] K.K.T. Phan, T. Truong, Y. Wang, B. Bhandari, Formation and stability of carbon dioxide nanobubbles for potential applications in food processing, Food Eng. Rev. 13 (2021) 3–14, https://doi.org/10.1007/s12393-020-09233-0.
[11] L. Zhou, S. Wang, L. Zhang, J. Hu, Generation and stability of bulk nanobubbles: a review and perspective, Curr. Opin. Colloid Interface Sci. 53 (2021) 101439, https://doi.org/10.1016/j.cocis.2021.101439.
[12] K. Ulatowski, P. Sobieszuk, A. Mróz, T. Ciach, Stability of nanobubbles generated in water using porous membrane system, Chem. Eng. Process. - Process Intesif. 136 (2019) 62–71, https://doi.org/10.1016/j.cep.2018.12.010.
[13] K. Yasuda, H. Matsushima, Y. Asakura, Generation and reduction of bulk nanobubbles by ultrasonic irradiation, Chem. Eng. Sci. 195 (2019) 455–461, https://doi.org/10.1016/j.ces.2018.09.044.
[14] Y. Tang, M. Zhang, J. Zhang, T. Lyu, M. Cooper, G. Pan, Reducing arsenic toxicity using the interfacial oxygen nanobubble technology for sediment remediation, Water Res. 205 (2021) 117657, https://doi.org/10.1016/j.watres.2021.117657.
[15] L. Ouyang, H.H.W.B. Hansen, H. Cha, X. Ji, J. Zhang, Q. Li, B.H. Tan, Q.T. Trinh, N.-T. Nguyen, H. An, A novel approach for nanobubble generation toward biomedical applications, Colloids Surf. A: Physicochem. Eng. Asp. 700 (2024) 134773, https://doi.org/10.1016/j.colsurfa.2024.134773.
[16] E.N. Harvey, A.H. Whiteley, W.D. McElroy, D.C. Pease, D.K. Barnes, Bubble formation in animals. II. Gas nuclei and their distribution in blood and tissues, J. Cell. Comp. Physiol. 24 (1944) 23–34, https://doi.org/10.1002/jcp.1030240103.
[17] Y. Wang, X. Li, S. Ren, H. Tedros Alem, L. Yang, D. Lohse, Entrapment of interfacial nanobubbles on nano-structured surfaces, Soft Matter 13 (2017) 5381–5388, https://doi.org/10.1039/C7SM01205E.
[18] E.P. Favvas, G.Z. Kyzas, E.K. Efthimiadou, A.C. Mitropoulos, Bulk nanobubbles, generation methods and potential applications, Curr. Opin. Colloid Interface Sci. 54 (2021) 101455, https://doi.org/10.1016/j.cocis.2021.101455.
[19] Y. Kuang, Y. Feng, H. Dong, L. Yang, Y. Zheng, Evolution process and stabilization mechanism of different gas nanobubbles based on improved statistical analysis, Nano Select 3 (2022) 1091–1101, https://doi.org/10.1002/nano.202100337.
[20] M. Kukizaki, M. Goto, Size control of nanobubbles generated from Shirasu-porous-glass (SPG) membranes, J. Membr. Sci. 281 (2006) 386–396, https://doi.org/10.1016/j.memsci.2006.04.007.
[21] A.A. Paknahad, I.O. Zalloum, R. Karshafian, M.C. Kolios, S.S.H. Tsai, High throughput microfluidic nanobubble generation by microporous membrane integration and controlled bubble shrinkage, J. Colloid Interface Sci. 653 (2024) 277–284, https://doi.org/10.1016/j.jcis.2023.09.066.
[22] H. Sharma, N. Nirmalkar, W. Zhang, Nanobubbles produced by nanopores to probe gas-liquid mass transfer characteristics, J. Colloid Interface Sci. 665 (2024) 274–285, https://doi.org/10.1016/j.jcis.2024.03.080.
[23] B.H. Tan, H. An, C.-D. Ohl, Surface nanobubbles are stabilized by hydrophobic attraction, Phys. Rev. Lett. 120 (2018) 164502, https://doi.org/10.1103/PhysRevLett.120.164502.
[24] B.H. Tan, H. An, C.-D. Ohl, Stability of surface and bulk nanobubbles, Curr. Opin. Colloid Interface Sci. 53 (2021) 101428, https://doi.org/10.1016/j.cocis.2021.101428.
[25] H. Peng, G.R. Birkett, A.V. Nguyen, Progress on the surface nanobubble story: what is in the bubble? Why does it exist? Adv. Colloid Interface Sci. 222 (2015) 573–580, https://doi.org/10.1016/j.cis.2014.09.004.
[26] A. Agrawal, J. Park, D.Y. Ryu, P.T. Hammond, T.P. Russell, G.H. McKinley, Controlling the location and spatial extent of nanobubbles using hydrophobically nanopatterned surfaces, Nano Lett. 5 (2005) 1751–1756, https://doi.org/10.1021/nl051103o.
[27] L. Bao, Z. Werbiuk, D. Lohse, X. Zhang, Controlling the growth modes of femtoliter sessile droplets nucleating on chemically patterned surfaces, J. Phys. Chem. Lett. 7 (2016) 1055–1059, https://doi.org/10.1021/acs.jpclett.6b00099.
[28] L. Wang, X. Wang, L. Wang, J. Hu, C.L. Wang, B. Zhao, X. Zhang, R. Tai, M. He, L. Chen, L. Zhang, Formation of surface nanobubbles on nanostructured substrates, Nanoscale 9 (2017) 1078–1086, https://doi.org/10.1039/C6NR06844H.
[29] L. Chen, Y. Deng, W. Han, C. Wang, D. Han, C. Feng, Effects of zeolite molecular sieve on the hydrocarbon adsorbent and diffusion performance of gasoline engine during cold start, Fuel 310 (2022) 122427, https://doi.org/10.1016/j.fuel.2021.122427.
[30] M.C. Duke, J.C.D. da Costa, D.D. Do, P.G. Gray, G.Q. Lu, Hydrothermally robust molecular sieve silica for wet gas separation, Adv. Funct. Mater. 16 (2006) 1215–1220, https://doi.org/10.1002/adfm.200500456.
[31] D.P. Erdosy, M.B. Wenny, J. Cho, C. DelRe, M.V. Walter, F. Jiménez-Ángeles, B. Qiao, R. Sanchez, Y. Peng, B.D. Polizzotti, M.O. de la Cruz, J.A. Mason, Microporous water with high gas solubilities, Nature 608 (2022) 712–718, https://doi.org/10.1038/s41586-022-05029-w.
[32] H.C. Foley, Carbogenic molecular sieves: synthesis, properties and applications, Microporous Mater. 4 (1995) 407–433, https://doi.org/10.1016/0927-6513(95)00014-Z.
[33] T.T. Moore, W.J. Koros, Gas sorption in polymers, molecular sieves, and mixed matrix membranes, J. Appl. Polym. Sci. 104 (2007) 4053–4059, https://doi.org/10.1002/app.25653.
[34] A. Schulte-Schulze-Berndt, K. Krabiell, Nitrogen generation by pressure swing adsorption based on carbon molecular sieves, Gas Sep. Purif. 7 (1993) 253–257, https://doi.org/10.1016/0950-4214(93)80026-S.
[35] E. Tooraji, A. Ghaemi, Nitrogen adsorption on molecular sieve zeolites: an experimental and modeling study, Iran. J. Oil Gas Sci. Technol. 9 (2020) 47–67, https://doi.org/10.22050/ijogst.2019.186102.1506.
[36] D.M. Ruthven, S. Farooq, Air separation by pressure swing adsorption, Gas Sep. Purif. 4 (1990) 141–148, https://doi.org/10.1016/0950-4214(90)80016-E.
[37] L. Kuraray Co., Carbon molecular sieves (CMS) and Nitrogen gas generator KURASEP™, https://www.kuraray-c.co.jp/en/products/device.html, 2024, (accessed 2024).
[38] R. Lin, A. Ladshaw, Y. Nan, J. Liu, S. Yiacoumi, C. Tsouris, D.W. DePaoli, L. L. Tavlarides, Isotherms for water adsorption on molecular sieve 3A: influence of cation composition, Ind. Eng. Chem. Res. 54 (2015) 10442–10448, https://doi.org/10.1021/acs.iecr.5b01411.
[39] L. Ouyang, Q. Zeng, N.-T. Nguyen, B.H. Tan, H. An, Destabilizing surface bubbles with excessive bulk oversaturation, Colloids Surf. A: Physicochem. Eng. Asp. 689 (2024) 133665, https://doi.org/10.1016/j.colsurfa.2024.133665.
[40] B.H. Tan, H. An, C.-D. Ohl, How bulk nanobubbles might survive, Phys. Rev. Lett. 124 (2020) 134503, https://doi.org/10.1103/PhysRevLett.124.134503.
[41] H.H.W.B. Hansen, H. Cha, L. Ouyang, J. Zhang, B. Jin, H. Stratton, N.-T. Nguyen, H. An, Nanobubble technologies: applications in therapy from molecular to cellular level, Biotechnol. Adv. 63 (2023) 108091, https://doi.org/10.1016/j.biotechadv.2022.108091.
[42] D. Park, Y. Ju, J.-H. Kim, H. Ahn, C.-H. Lee, Equilibrium and kinetics of nitrous oxide, oxygen and nitrogen adsorption on activated carbon and carbon molecular

sieve, Sep. Purif. Technol. 223 (2019) 63–80, https://doi.org/10.1016/j.seppur.2019.04.051.
[43] H. Qinglin, S.M. Sundaram, S. Farooq, Revisiting transport of gases in the micropores of carbon molecular sieves, Langmuir 19 (2003) 393–405, https://doi.org/10.1021/la026451+.
[44] T. Yamashita, K. Ando, Aeration of water with oxygen microbubbles and its purging effect, J. Fluid Mech. 825 (2017) 16–28, https://doi.org/10.1017/jfm.2017.376.
[45] H. Tarábková, P. Janda, Effect of graphite aging on its wetting properties and surface blocking by gaseous nanodomains, Langmuir 39 (2023) 14154–14161, https://doi.org/10.1021/acs.langmuir.3c02151.
[46] M.M. Dubinin, Water vapor adsorption and the microporous structures of carbonaceous adsorbents, Carbon 18 (1980) 355–364, https://doi.org/10.1016/0008-6223(80)90007-X.
[47] S.K. Verma, P.L. Walker, Carbon molecular sieves with stable hydrophobic surfaces, Carbon 30 (1992) 837–844, https://doi.org/10.1016/0008-6223(92)90004-G.
[48] N.D. Petsev, L.G. Leal, M.S. Shell, Universal gas adsorption mechanism for flat nanobubble morphologies, Phys. Rev. Lett. 125 (2020) 146101, https://doi.org/10.1103/PhysRevLett.125.146101.
[49] B.H. Tan, H. An, C.-D. Ohl, Comment on universal gas adsorption mechanism for flat nanobubble morphologies', Phys. Rev. Lett. 129 (2022) 099601 https://doi.org/10.1103/PhysRevLett.129.099601.
[50] D.H. Everett, J.C. Powl, Adsorption in slit-like and cylindrical micropores in the Henry's law region. A model for the microporosity of carbons, J. Chem. Soc., Faraday Trans. 1 72 (1976) 619–636, https://doi.org/10.1039/F19767200619.
[51] N. Khatri, K.K. Khatri, A. Sharma, Enhanced energy saving in wastewater treatment plant using dissolved oxygen control and hydrocyclone, Environ. Technol. Innov. 18 (2020) 100678, https://doi.org/10.1016/j.eti.2020.100678.
[52] Z.-J. Wang, H.-Y. Wang, Y.-L. Li, J. Chu, M.-Z. Huang, Y.-P. Zhuang, S.-L. Zhang, Improved vitamin B12 production by step-wise reduction of oxygen uptake rate under dissolved oxygen limiting level during fermentation process, Bioresour. Technol. 101 (2010) 2845–2852, https://doi.org/10.1016/j.biortech.2009.10.048.